Journal of Catalysis **189,** 16–30 (2000)
Article ID jcat.1999.2699, available online at http://www.idealibrary.com on IDEAL®

Theoretical Studies of Stability and Reactivity of CH_x Species on Ni(111)

R. M. Watwe,*,† H. S. Bengaard,‡ J. R. Rostrup-Nielsen,† J. A. Dumesic,* and J. K. Nørskov‡

*Department of Chemical Engineering, University of Wisconsin—Madison, Madison, Wisconsin 53706; ‡Center for Atomic-Scale Materials Physics, Technical University of Denmark, DK-2800 Lyngby, Denmark; and †Haldor Topsøe Research Laboratories, Nymøllevej 55, DK-2800 Lyngby, Denmark

Received April 19, 1999; revised September 9, 1999; accepted September 28, 1999

Periodic infinite plane wave slab calculations were performed, in conjunction with density functional theory and ultrasoft pseudopotentials to study the adsorption of CH_x ($x = 1, 2, 3$) species on the Ni(111) surface. The potential energy diagram is presented for the overall reaction of surface carbon with dihydrogen to methane or, equivalently, the conversion of methane to surface carbon, including all adsorbed intermediates and transition states. All CH_x intermediates prefer threefold sites. The transition states involve the formation of C–H bonds on top of a Ni atom, with the reaction coordinate being primarily a C–H stretch. The calculated activation energies to form the C–H bond are near 70–85 kJ/mol for different CH_x species. To illustrate the new possibilities offered by detailed potential energy diagrams, the results from the quantum chemical calculations are combined with experimental results in the literature to make initial estimates of kinetic parameters involved in the methanation of CO over nickel. Sensitivity analyses in this region of parameter space are used to assess the effects of these kinetic parameters on the overall rate of methanation. A good description of the experimental methanation reaction kinetics (D. W. Goodman *et al., J. Catal.* 63, 226 (1980)) is achieved by adjusting the sensitive kinetic parameters within reasonable ranges. The kinetic analyses shows that adsorbed CO and CH are the most abundant species on the surface, and the energies of the transition states to form methyl species from methylene species and to form methane from methyl species appear to control the rate of the overall reaction. © 2000 Academic Press

INTRODUCTION

Surface reactions of methane on nickel surfaces have been studied extensively, since these reactions are involved in industrially important reactions, such as steam reforming of methane and methanation of carbon monoxide (2, 3). For example, an important industrial application of the methanation reaction is the removal of trace amounts of CO from H_2-rich feed gases, while steam reforming is used to produce synthesis gas from methane.

The sequential dehydrogenation of methane on Ni surface constitutes an important part of the reaction mechanism for the methanation and steam reforming reactions. Many experimental and theoretical studies have been conducted of CH_x species adsorbed on Ni surfaces (4–11). All CH_x fragments have been observed on Ni(111) using SIMS (11), while the existence of adsorbed CH_3 and CH species was reported using HREELS (12). Kinetic studies have shown methanation of CO to be a structure-insensitive reaction (1, 13). Theoretical studies of methane dissociation on Ni have been carried out using mainly the cluster approach to predict the relative stabilities of the various adsorbed CH_x species (4, 6, 8, 10).

In the present paper, we describe our theoretical investigations using density functional theory of the stability and reactivity of CH_x species on Ni(111). The following steps were considered in our work:

$$C^* + H^* = CH^* + *$$
$$CH^* + H^* = CH_2^* + *$$
$$CH_2^* + H^* = CH_3^* + *$$
$$CH_3 + H^* = CH_4 + 2^*.$$

In contrast to earlier reported theoretical studies on this system, we have used the slab approach, which rigorously accounts for the true electronic structure and extended field effects for a well-defined surface. Periodic infinite plane wave slab calculations were performed in conjunction with the ultrasoft pseudopotentials. In addition to calculating the energetics of stable CH_x species on Ni(111), we also have calculated the activation barriers for C–H bond activation of these species.

An important application of knowing the energetics of surface species is formulating a description of reaction kinetics involving those surface species. We show in the present paper how the theoretical results from this study and available experimental data can be consolidated to form a kinetic model for methanation over nickel, and we use this model to describe the pressure and temperature dependence of the methanation rate measured experimentally by Goodman *et al.* on Ni(100) (1). This reaction analysis is conducted using De Donder relations (14), by which the overall rate of the reaction is expressed in terms of quasi-equilibria between the reactants and/or products of

0021-9517/00 $35.00

overall reaction with the transition states and most abundant surface species of the reaction scheme. We first combine the results from our quantum chemical calculations with experimental results in the literature to make initial estimates for all kinetic parameters. We subsequently conduct sensitivity analyses in this region of parameter space to assess the effects of these kinetic parameters on the overall rate of methanation, and we then adjust the values of the sensitive kinetic parameters within reasonable ranges to achieve a description of the experimental methanation reaction kinetics.

CALCULATIONS

We have primarily used a two-layer slab of Ni(111) periodically repeated in a super cell geometry with four equivalent layers of vacuum between any two successive metal slabs. We have also used four-layer slabs to investigate the effect of the slab thickness on the calculated energetics. The calculated equilibrium lattice constant was 3.52 Å. A 2×2 unit cell was used to study the adsorption of various species, corresponding to one-fourth monolayer coverage. Adsorption occurs on one side of the slab to avoid errors originating from the spurious interactions of adsorbates through the slab. Usually, the adsorbate atoms were allowed to relax, while the surface layer was kept fixed, but we also investigated the effect of surface atom relaxations in one case. Ionic cores are described by ultrasoft pseudopotentials (15) and the Kohn–Sham one-electron valence states are expanded in a basis of plane waves with kinetic energies below 25 Ry. The surface Brillouin zone is sampled at 18 special k points. The exchange-correlation energy and potential are described by the generalized gradient approximation (PW91) (16, 17). The self-consistent PW91 density is determined by iterative diagonalization of the Kohn–Sham Hamiltonian, Fermi population of the Kohn–Sham states ($k_BT = 0.1$ eV), and Pulay mixing of the resulting electronic density (18). All total energies have been extrapolated to $k_BT = 0$ eV. In a previous study, use of a recently developed exchange-correlation energy functional, denoted as RPBE, was shown to result in better chemisorption energies of atoms and molecules on transition metal surfaces (19). Hence, we report non-self-consistently determined chemisorption energies for this RPBE functional. These values are used for further analysis of the CO methanation reaction. For comparison, we also report the self-consistently determined energies for the PW-91 functional, which generally overpredict the binding energies. We note that the variational principle of density functional theory guarantees that the density and the potential output to the Kohn–Sham Hamiltonian may be varied independently while giving rise to errors in the total energy that are second order in the variations of the density and potential from their ground state values. We have used the nonspin polarized version of the exchange-correlation functional. Generally adsorbates like hydrogen lower the spin of nickel and thus spin polarization is less important for the adsorbed phase. The additional (small) stabilization of the clean nickel surface due to magnetic ordering is not taken into account and thus we may overestimate the binding energies.

Isolated H_2 and CH_4 Molecules

We have used a large super cell of 10-Å lattice constant to calculate the energy of isolated H_2 molecules. The calculated bond length is 0.75 Å, which is in agreement with the experimental value of 0.74 Å. For methane, we have used a super cell with a lattice constant of 10 Å. The calculated C–H bond length is 1.10 Å, in agreement with the experimental value of 1.09 Å. The calculated energy to dissociate CH_4 into a carbon atom and two dihydrogen molecules is 833 kJ/mol, which is comparable to the experimental value of 841 kJ/mol (20). This experimental value does not contain zero point energy contribution, which makes it a valid comparison to the calculated value at 0 K. To test the adequacy of the super cell and basis set, we have also determined the properties of methane in the same super cell as used for the surface calculations. Specifically, we put the methane molecule at the center of the vacuum region between two successive nickel slabs. We find that the energy calculated by this approach is same as that obtained by using a large super cell.

Hydrogen on Ni(111)

Hydrogen adsorbs on threefold sites on Ni(111). The calculated energy of dissociative adsorption of a dihydrogen molecule is −86 kJ/mol on a threefold hollow (fcc) site. Experimentally, H_2 dissociation is found to be exothermic by 95 kJ/mol (21). The vertical distance of adsorbed H atom above the Ni surface is calculated to be 0.91 Å, which is shorter than the experimental value of 1.15 ± 0.05 Å (22). Similar findings were reported earlier where the difference in the bond length was attributed to the neglect of spin polarization effects in the calculated value. The Ni–H bond length is 1.70 Å, while the experimental value is 1.84 ± 0.06 Å (23).

We have also performed calculations on a four-layer Ni slab. The dissociation of H_2 is found to be exothermic by 88 kJ/mol on a four-layer slab, compared to 86 kJ/mol on a two-layer slab. Hence, we see no significant effect of the slab thickness on the calculated energy changes for dissociation of H_2. When the H atom is adsorbed on a hcp site on a two-layer Ni slab, the H_2 dissociation is found to be exothermic by 77 kJ/mol, indicating a slight preference for an fcc site over a hcp site for H adsorption.

Carbon on Ni(111)

Carbon is found to prefer a threefold site in accord with earlier reports (24). The calculated binding energy of

carbon is 613 kJ/mol on a fcc site. The equilibrium distance between carbon and the Ni surface is 1.02 Å and the Ni–C bond length is 1.76 Å. There is no difference in the binding energies for carbon between fcc and hcp sites. Four-layer slab calculations showed no effect of the slab thickness on the binding energy and structure of adsorbed carbon. We have also studied the effect of vertical relaxation of the surface Ni atoms on the binding energy of carbon. For the four-layer nickel slab with relaxation allowed for the uppermost layer, the interplanar distance between the uppermost layer and the next layer contracted to 2.01 Å from its bulk value of 2.03 Å. The adsorbed carbon atom pulls out the three Ni atoms bonded to it while carbon pushes the fourth atom in the unit cell toward the inner Ni layer. The corresponding interplanar distances are 2.11 and 1.99 Å. A recent theoretical study also showed a slight inward relaxation of the topmost Ni layer and an outward relaxation of the topmost layer upon adsorption of carbon (24). We find that this relaxation does not change the binding energy of carbon. We note that an STM study of carbon-induced structures on Ni(111) showed evidence for a carbidic-phase clock reconstruction (25), and a separate theoretical study has shown that a similar carbon-induced clock reconstruction on Ni(100) stabilizes the adsorbate by approximately 20 kJ/mol.

CH on Ni(111)

We find that the three-fold hollow site is the stable site for CH (methylidyne) adsorption on Ni(111), in agreement with experimental observations (12) (Fig. 1). Adsorbed methylidyne has C_{3v} symmetry. The carbon atom is located 1.14 Å above the Ni surface with the Ni–C bond length being 1.83 Å. The C–H bond length is 1.10 Å, which is same as that calculated for isolated CH_4 molecules. This observation suggests that CH is sp^3 hybridized on the Ni surface. We have calculated the C–H stretching frequency to be 3035 cm^{-1}, which is in agreement with the experimental value of 2970 cm^{-1} for CH adsorbed on Ni(111) (12). We find that the reaction $CH_4 = CH(ads) + 3H(ads)$ is exothermic by 5 kJ/mol.

CH_2 on Ni(111)

We have investigated two types of sites for CH_2(methylene) adsorption on Ni(111). Figure 2a shows methylene adsorbed on a bridge site. For the tetravalency of C to be preserved, CH_2 should adsorb on a bridge site; however, we find that CH_2 prefers by 20 kJ/mol a threefold hollow site, as shown in Fig. 2b. In the bridge site, the Ni–C bond length is 1.89 Å and C–H bond length is 1.11 Å. In the three-fold site, the C atom is located nearly symmetrically at the center, at a distance of 1.29 Å from the surface. The Ni–C bond length is approximately 1.93 Å. The two C–H bonds are unequal in length, with the longer C–H bond being 1.15 Å. The H atom in this C–H bond lies over a Ni atom, with the Ni–H distance being 1.83 Å. This latter value can be compared to 1.70 Å for adsorbed H, as described earlier. This short Ni–H distance indicates a significant Ni–H interaction, which leads to the lengthening of this C–H bond to 1.15 Å from its normal value of 1.10 Å. The other H atom points toward a bridge site, and the Ni–H distance is 2.46 Å. Hence there is no Ni–H interaction for this H atom and the C–H bond length is 1.10 Å. We find that the reaction $CH_4 = CH_2(ads) + 2H(ads)$ is endothermic by 38 kJ/mol.

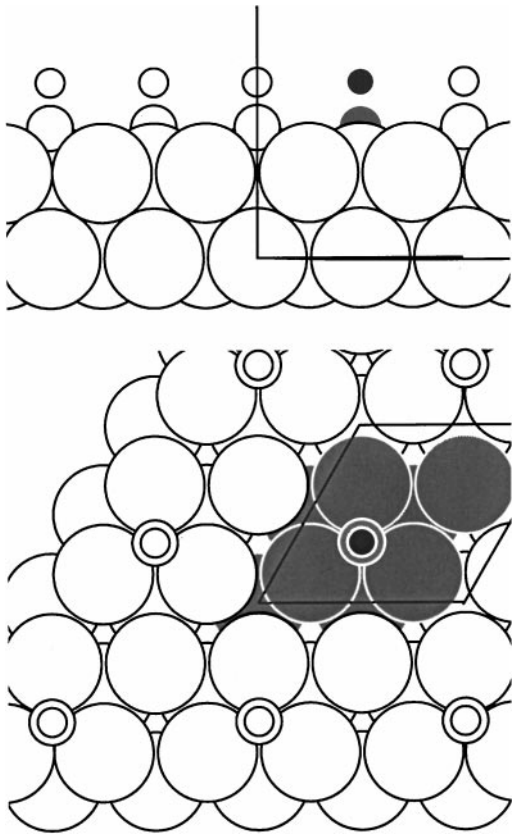

FIG. 1. Side and top view of CH (methylidyne) species on Ni(111) surface. The shaded metal atoms illustrate the unit cell used. Large shaded circle denotes a Ni atom. Smaller shaded circle denotes a carbon atom while a dark small circle represents a hydrogen atom.

CH_3 on Ni(111)

Methyl species (CH_3) are found to adsorb on threefold hollow sites with H atoms pointing toward Ni atoms, as shown in Fig. 3a. This observation is in agreement with previous experimental and theoretical studies (9, 12). The adsorbed methyl species has C_{3v} symmetry. The C atom is located 1.50 Å above the surface, and the Ni–C bond length is 2.08 Å. The H–C–H angle is 106°, compared to 109.5° in CH_4. The C–H bond length is 1.12 Å, compared to 1.10 Å in CH_4. The H atoms are located nearly on top of Ni atoms with the Ni–H distance being 1.97 Å. This fairly short distance suggests a Ni–H interaction, which results in

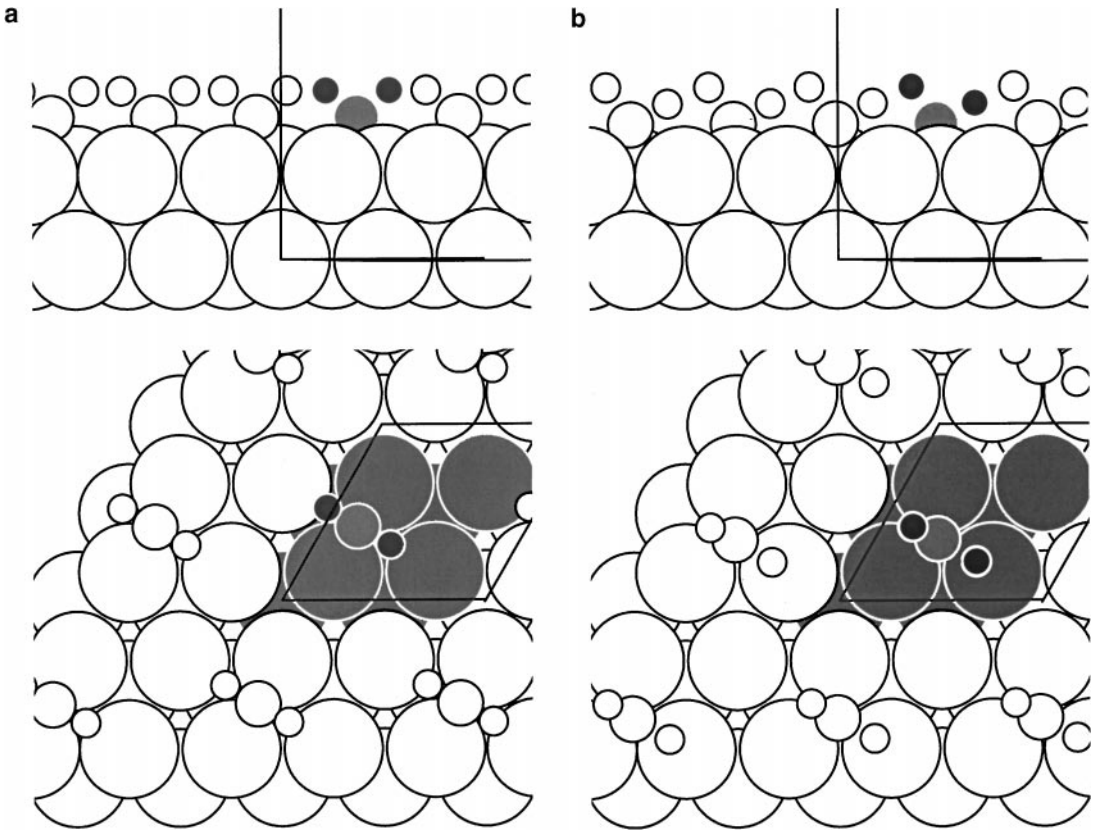

FIG. 2. Side and top view of CH_2 (methylene) species on a (a) bridge site and a (b) threefold site.

elongated C–H bonds. We have calculated the symmetric C–H stretching frequency to be 2730 cm^{-1} which is in agreement with the experimental value of 2655 cm^{-1}. We have performed calculations for CH_3 adsorbed on a four-layer Ni slab and found no difference in the calculated structure and energetics compared to the two-layer slab.

We have investigated two other adsorption configurations for methyl species. Figure 3b shows the configuration where H atoms point toward bridge sites between two Ni atoms. In this configuration, the C atom is located symmetrically in the threefold site at 1.65 Å from the surface. The Ni–C bond length is 2.19 Å. The C–H bond length is 1.10 Å, since the H atom is located at a long distance of 2.43 Å from Ni. This configuration is less stable than that of Fig. 3a by 33 kJ/mol, suggesting a hindered methyl rotation. The other type of site for methyl adsorption is an atop site, as shown in Fig. 3c. The C atom is located at 1.96 Å above the Ni atom. This configuration is less stable than that of Fig. 3a by 20 kJ/mol.

We note that only the most stable methyl configuration has an elongated C–H bond, which results in the experimentally observed soft C–H stretching frequency. We find that the reaction $CH_4 = CH_3(ads) + H(ads)$ is endothermic by 41 kJ/mol, for the most stable configuration of methyl adsorption.

Location of Transition States

We have conducted several constrained optimizations of the adsorbate to map the reaction coordinate. We assume that the reaction coordinate consists primarily of C–H bond elongation. We fix the value of the C–H bond length and optimize the adsorbate on the Ni surface. After a series of such calculations, we locate an approximate maximum in the energy versus C–H bond length. We also verify that the slope of the forces changes its sign at the maximum, verifying that we have located the transition state connecting the desired reactants and products.

The approximate transition state structure for methane activation ($2^* + CH_4 = {}^*CH_3 + {}^*H$) is shown in Fig. 4a. A similar transition state for CH_4 dissociating over the top of a Ni atom has been examined in detail in our earlier report (7). The C atom is located above the Ni atom at a distance of 2.07 Å. The Ni–H bond length is 1.54 Å. The forward activation energy is calculated to be 127 kJ/mol.

The approximate transition state structure is shown in Fig. 4b for methyl dehydrogenation ($* + {}^*CH_3 = {}^*CH_2 + {}^*H$). The reaction coordinate is assumed to be primarily the C–H bond stretch over the top of a Ni atom. The C–H bond stretches to around 1.77 Å when the bond breaks. The H atom in this C–H bond is located at 1.44 Å over the Ni

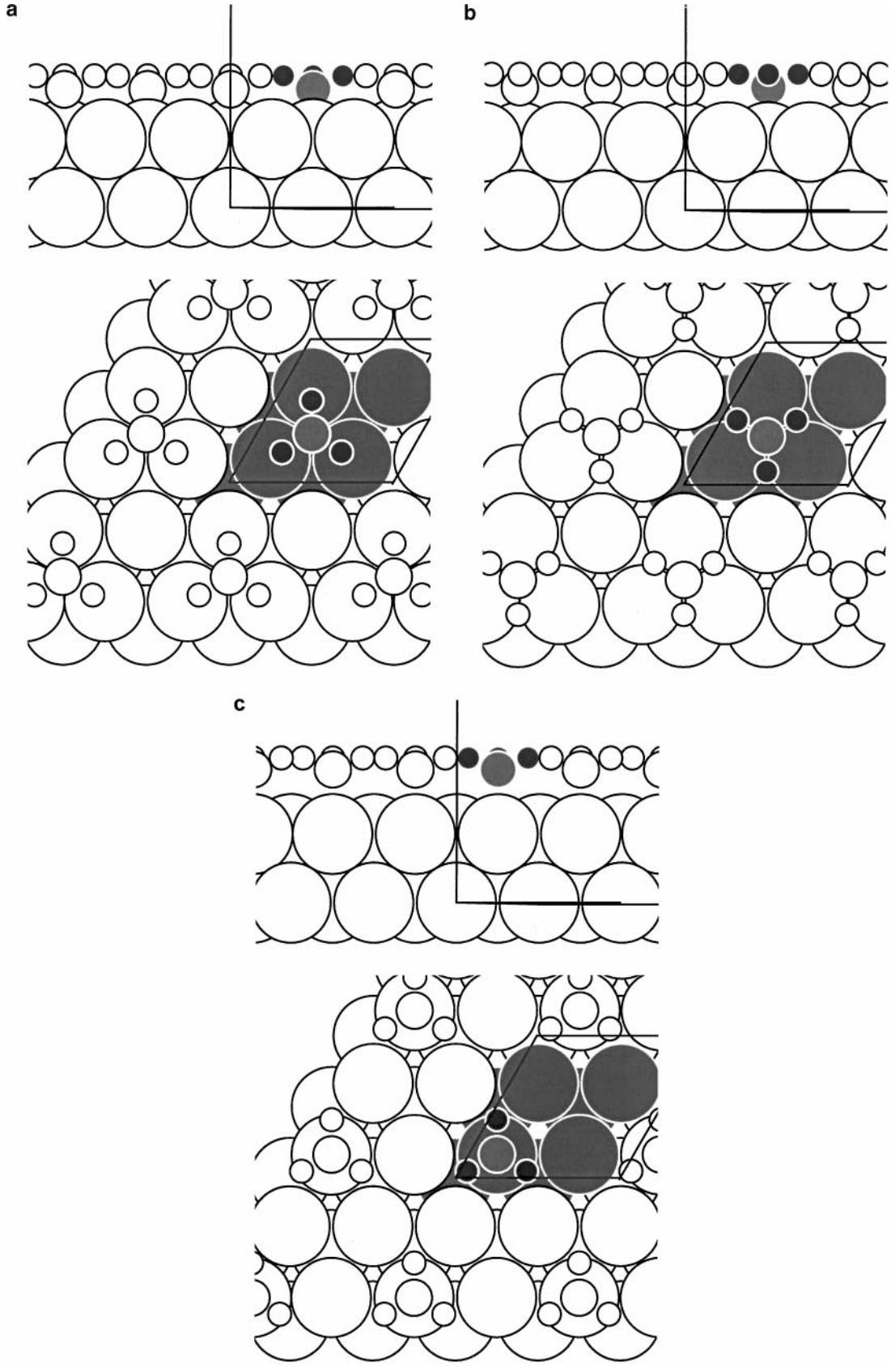

FIG. 3. Side and top view of (a) most stable configuration of CH_3 (methyl) species, (b) methyl species where H atoms point toward bridge sites, and (c) methyl species on an atop site.

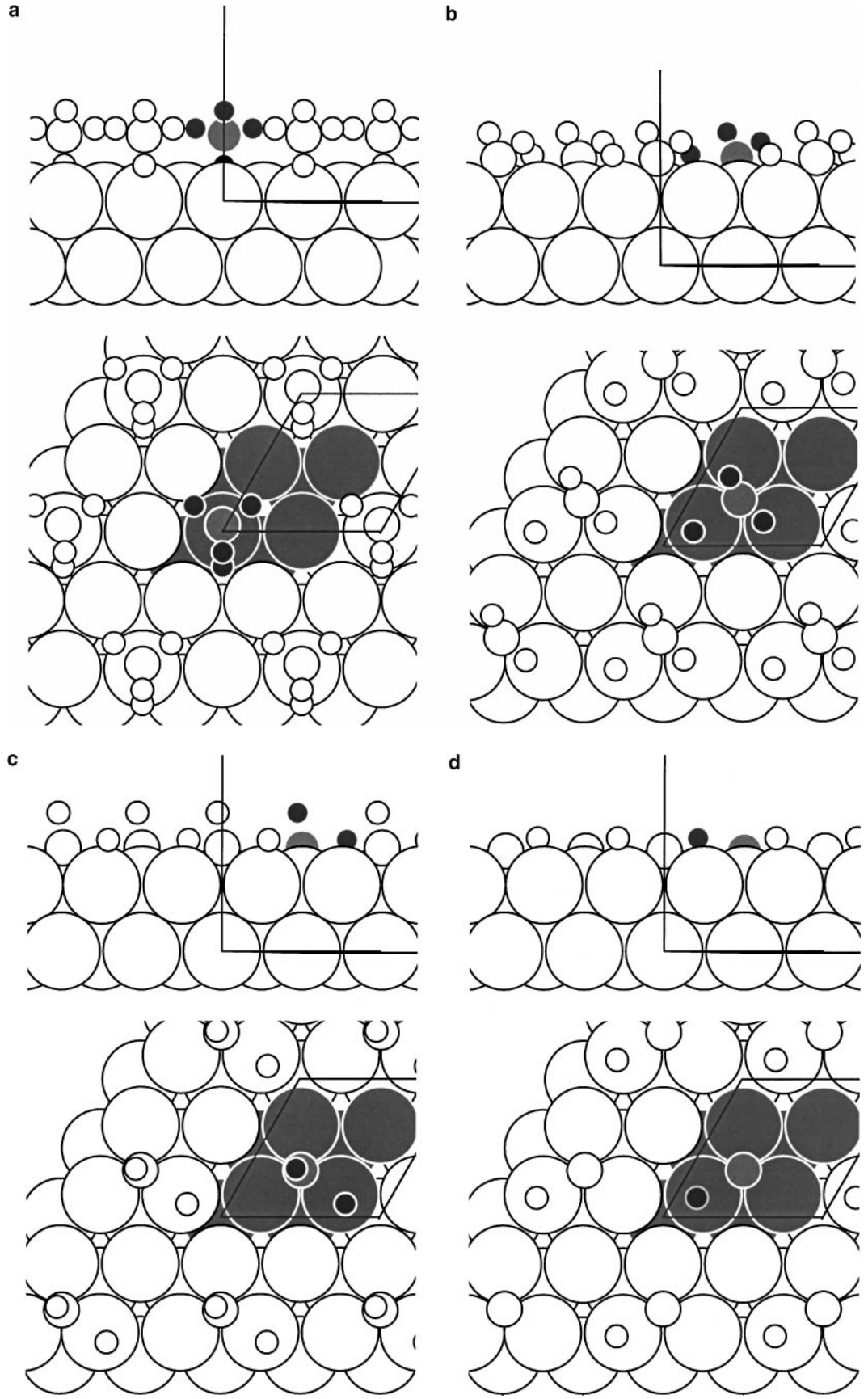

FIG. 4. Side and top view of approximate transition state for the formation of (a) methane from methyl, (b) methyl from methylene, (c) methylene from methylidyne, and (d) methylidyne from adsorbed carbon.

surface, and the Ni–H bond distance is 1.50 Å. The C atom remains in the threefold hollow site during this elementary step. The products are methylene species adsorbed on a threefold fcc site and a H atom adsorbed in an adjacent threefold hcp site. The interaction for this product configuration is repulsive by 22 kJ/mol compared to adsorbates infinitely separated on the surface. The calculated activation energy for this elementary step in forward direction is 68 kJ/mol.

The approximate transition state structure for methylene dehydrogenation ($* + {}^*CH_2 = {}^*CH + {}^*H$) is shown in Fig. 4c. As noted earlier, an adsorbed CH_2 species has two unequal C–H bond lengths. We have chosen to investigate the dissociation of the longer C–H bond, since one can expect this process to be less activated compared to dissociation of the shorter C–H bond. In addition, the longer C–H bond lies more parallel to the surface than the shorter one. In the approximate transition state structure, the C–H bond is stretched to 1.60 Å (Fig. 4c). This H atom is located at 1.50 Å above the surface, with the Ni–H bond distance also being 1.50 Å. The products for this elementary step are methylidyne species adsorbed on threefold fcc site and a H atom adsorbed in an adjacent hcp site. The interaction for this product configuration is repulsive by 12 kJ/mol compared to adsorbates infinitely separated on the surface. The calculated activation energy for this elementary step in the forward direction is 28 kJ/mol. This step is the least activated elementary step among the four steps that we have investigated in this paper.

The approximate transition state structure for methylidyne dehydrogenation ($* + {}^*CH = {}^*C + {}^*H$) is shown in Fig. 4d. The C–H bond is oriented perpendicular to the Ni surface. In the approximate transition state structure, the C atom is located in the threefold hollow site, the H atom is located at 1.47 Å above the surface, and the Ni–H bond distance is 1.49 Å (Fig. 4d). The C–H bond length is 1.77 Å. The products for this elementary step are C adsorbed on fcc site and a H atom adsorbed in an adjacent hcp site. The interaction for this product configuration is repulsive by 21 kJ/mol compared to adsorbates infinitely separated on the surface. The calculated activation energy for this elementary step in the forward direction is 139 kJ/mol. This step has the highest activation barrier of the four elementary steps. The C–H bond dissociation involves the C–H bond lying approximately parallel to the surface, which requires the C–H bond to bend from its equilibrium position. The other two species, namely the methyl and methylene, have their C–H bonds more parallel to the surface.

KINETICS OF CO METHANATION

Rationale for Kinetic Model

The following reaction scheme was used to construct a kinetic model for the methanation reaction:

$$H_2 + 2^* = 2H^* \quad \text{Step 1}$$

$$CO + * = CO^* \quad \text{Step 2}$$

$$CO^* + * = C^* + O^* \quad \text{Step 3}$$

$$C^* + H^* = CH^* + * \quad \text{Step 4}$$

$$CH^* + H^* = CH_2^* + * \quad \text{Step 5}$$

$$CH_2^* + H^* = CH_3^* + * \quad \text{Step 6}$$

$$CH_3^* + H^* = CH_4 + 2^* \quad \text{Step 7,}$$

where $*$ represents a surface site. This reaction scheme is based on the scheme used by Alstrup (26). In our kinetic analyses, we have assumed that steps 1 and 2 for H_2 and CO adsorption are quasi-equilibrated, step 3 for CO dissociation is irreversible owing to rapid removal of surface O by hydrogenation and desorption of H_2O, and step 7 for desorption of methane is irreversible. These assumptions are also in accord with the work of Alstrup (26).

The prediction of reaction kinetics from a reaction scheme requires estimates of kinetic parameters for all of the reaction steps; however, it is typically found that a limited number of these kinetic parameters are kinetically significant. Thus, the kinetic analysis begins by making estimates of all kinetic parameters, and then conducting sensitivity analyses of the effects on the reaction kinetics of changing individual kinetic parameters. Importantly, the rate expression typically involves products of individual kinetic parameters, and a combined kinetic parameter composed of a product of individual kinetic parameters provides a better basis for sensitivity analyses, compared to sensitivity analyses of the effects of the individual kinetic parameters. In this respect, it is necessary to identify appropriate combinations of individual kinetic parameters to simplify sensitivity analyses.

Another situation where combination of kinetic parameters is appropriate involves the reference state for the definition of activation energies for surface reactions. For example, we may define the energy of the surface activated complex for a particular step relative to the adsorbed reactants of that step. In this case, however, the kinetic model may become sensitive to the energy of the activated complex and to the energy of the adsorbed reactants, and we have a situation where it is appropriate to combine these effects by defining the energy of the activated complex relative to the reactants in the gas phase.

It has been shown elsewhere that a convenient means of achieving effective combinations of kinetic parameters is provided by using De Donder relations to derive the rate expression from a reaction scheme of elementary steps (14). In short, De Donder relations are used to express the overall rate of the reaction in terms of quasi-equilibria between the reactants and/or products of overall reaction with the transition states of the elementary steps, and the fraction of the surface that is available for reaction is expressed by

equilibria between the reactants and/or of overall reaction with the abundant surface adsorbed species. This formalism for kinetic analyses is particularly well suited for cases where the properties of the activated complexes and surface adsorbed species have been estimated by quantum chemical calculations.

In the following section, we use De Donder relations to derive the rate expression for the methanation reaction in terms of combined, quasi-equilibria with gaseous H_2 and CO. We then combine the results from our quantum chemical calculations with experimental results in the literature to make initial estimates for all of the combined kinetic parameters. This initial estimation of kinetic parameters is critical, since it is important to start kinetic analyses in a reasonable region of parameter space. We next conduct sensitivity analyses in this region of parameter space to assess the effects of these combined kinetic parameters on the overall rate of methanation. Finally, we adjust the values of the sensitive kinetic parameters within reasonable ranges to achieve a description of the experimental methanation reaction kinetics reported by Goodman *et al.* (1).

Derivation of Methanation Rate Expression Using De Donder Relations

According to De Donder (27–29), we write the net rate for elementary step i in terms of the forward rate of the step, $\boldsymbol{r}_i$, and the affinity for the step, A_i,

$$r_i = \boldsymbol{r}_i \left[1 - \exp\left(\frac{-A_i}{RT}\right)\right], \qquad [1]$$

where the affinity is equal to minus the change in the Gibbs free energy with respect to the extent of reaction. The affinity, A_i, is expressed in terms of the standard state Gibbs free energies, G_j°, and the activities, a_j, of the j reactants and products of the step,

$$A_i = -\sum_j \upsilon_{ij} G_j = -\sum_j \upsilon_{ij}\left[G_j^{\circ} + RT\ln(a_j)\right], \qquad [2]$$

where υ_{ij} are the stoichiometric coefficients for the j reactants and products of step i. This expression can be written in terms of the equilibrium constant for the step, $K_{i\mathrm{eq}}$,

$$\exp\left(\frac{-A_i}{RT}\right) = \frac{\prod_j a_j^{\upsilon_{ij}}}{K_{i\mathrm{eq}}}, \qquad [3]$$

since the equilibrium constant is determined by the change in the standard state Gibbs free energies:

$$K_{i\mathrm{eq}} = \exp\left[\frac{-\sum_j \upsilon_{ij} G_j^{\circ}}{RT}\right]. \qquad [4]$$

For convenience, we may define a dimensionless variable, z_i, equal to the exponential of $-A_i/RT$:

$$z_i = \exp\left(\frac{-A_i}{RT}\right) = \frac{\prod_j a_j^{\upsilon_{ij}}}{K_{i\mathrm{eq}}}. \qquad [5]$$

The value of z_i approaches zero as step i becomes irreversible, and as z_i approaches unity as step i becomes quasi-equilibrated. Therefore this value of z_i may be termed as the reversibility of step i.

For quasi-equilibrated steps 1 and 2 we can write

$$\theta_{\mathrm{H}} = \sqrt{K_1 P_{\mathrm{H}_2}}\,\theta_* \qquad [6]$$

$$\theta_{\mathrm{CO}} = K_2 P_{\mathrm{CO}}\theta_*. \qquad [7]$$

Note that the values of z_1 and z_2 are equal to unity for these quasi-equilibrated steps.

For nonequilibrated steps 4, 5, and 6 we write

$$\theta_{\mathrm{CH}} = K_4 z_4 \sqrt{K_1 P_{\mathrm{H}_2}}\,\theta_{\mathrm{C}} \qquad [8]$$

$$\theta_{\mathrm{CH}_2} = K_4 K_5 z_4 z_5 \left(K_1 P_{\mathrm{H}_2}\right)\theta_{\mathrm{c}} \qquad [9]$$

$$\theta_{\mathrm{CH}_3} = K_4 K_5 K_6 z_4 z_5 z_6 \left(K_1 P_{\mathrm{H}_2}\right)^{3/2}\theta_{\mathrm{c}}. \qquad [10]$$

And the net rates for steps 3–7 can be written as

$$r_3 = K_2 k_3 P_{\mathrm{CO}}\theta_*^2 \qquad [11]$$

$$r_4 = \left(\sqrt{K_1} k_4\right)\sqrt{P_{\mathrm{H}_2}}\,\theta_{\mathrm{c}}\theta_*(1 - z_4) \qquad [12]$$

$$r_5 = (K_1 K_4 k_5) z_4 P_{\mathrm{H}_2}\theta_{\mathrm{c}}\theta_*(1 - z_5) \qquad [13]$$

$$r_6 = \left(K_1^{3/2} K_4 K_5 k_6\right) z_4 z_5 P_{\mathrm{H}_2}^{3/2}\theta_{\mathrm{c}}\theta_*(1 - z_6) \qquad [14]$$

$$r_7 = \left(K_1^2 K_4 K_5 K_6 k_7\right) z_4 z_5 z_6 P_{\mathrm{H}_2}^2\theta_{\mathrm{c}}\theta_*. \qquad [15]$$

We have set the value of z_7 to zero, since this step has been assumed to be irreversible. We now use transition state theory to express each rate constant k_i as

$$k_i = \nu^{\ddagger} K_i^{\ddagger}, \qquad [16]$$

where K_i is the equilibrium constant for the formation of the activated complex from the reactants of step i, $\nu^{\ddagger}$ is a frequency factor equal to $k_{\mathrm{B}}T/h$, k_{B} is the Boltzmann constant, and h is Planck's constant. We note that since conventional transition-state theory assumes quasi-equilibrium between the reactants and the activated complex, this approach fails when the activation barrier is typically lower than 5 RT (30, 31). In addition, this approach is not valid for situations where multiple crossings through the transition state take place or where quantum mechanical tunneling is important.

Now we define combined, quasi-equilibrium parameters $K_{\mathrm{act},i}$ as follows:

$$K_{\text{act3}} = \nu^{\ddagger} K_2 K_3^{\ddagger} \quad [17]$$

$$K_{\text{act4}} = \nu^{\ddagger} K_1^{0.5} K_4^{\ddagger} \quad [18]$$

$$K_{\text{act5}} = \nu^{\ddagger} K_1 K_4 K_5^{\ddagger} \quad [19]$$

$$K_{\text{act6}} = \nu^{\ddagger} K_1^{1.5} K_4 K_5 K_6^{\ddagger} \quad [20]$$

$$K_{\text{act7}} = \nu^{\ddagger} K_1^{2} K_4 K_5 K_6 K_7^{\ddagger}. \quad [21]$$

We note that a product of equilibrium constants for steps i can be expressed by a single equilibrium constant for an overall reaction that is a linear combination of these individual steps i. Therefore, it is apparent that kinetic parameters K_{act3} through K_{act7} are controlled by the following combined quasi-equilibria:

$$K_{\text{act3}}: \quad \text{CO} + 2^* = \text{Act}_3^{\ddagger}$$

$$K_{\text{act4}}: \quad * + 0.5\,\text{H}_2 + \text{C}^* = \text{Act}_4^{\ddagger}$$

$$K_{\text{act5}}: \quad * + \text{H}_2 + \text{C}^* = \text{Act}_5^{\ddagger}$$

$$K_{\text{act6}}: \quad * + 1.5\,\text{H}_2 + \text{C}^* = \text{Act}_6^{\ddagger}$$

$$K_{\text{act7}}: \quad * + 2\,\text{H}_2 + \text{C}^* = \text{Act}_7^{\ddagger},$$

where $\text{Act}_i^{\ddagger}$ is the activated complex involved in step i.

Next, to determine the fraction of the surface that is available for the catalytic reaction, θ_*, we write a site balance,

$$1 = \theta_* + \theta_{\text{H}} + \theta_{\text{CO}} + \theta_{\text{c}} + \theta_{\text{CH}} + \theta_{\text{CH}_2} + \theta_{\text{CH}_3}, \quad [22]$$

which can be written as

$$1 = \theta_*\left(1 + \sqrt{K_1 P_{\text{H}_2}} + K_2 P_{\text{CO}}\right) + \theta_{\text{c}}\left(1 + \sqrt{K_1} K_4 P_{\text{H}_2}^{1/2} z_4 + K_1 K_4 K_5 P_{\text{H}_2} z_4 z_5 + K_1^{3/2} K_4 K_5 K_6 P_{\text{H}_2}^{3/2} z_4 z_5 z_6\right). \quad [23]$$

It is apparent that the fractional coverage θ_* is controlled by equilibrium constants K_1 and K_2 for adsorption of H^*, CO^*, and the following combined equilibrium constants for adsorption of CH^*, CH_2^*, and CH_3^*:

$$K_{\text{CH}} = \sqrt{K_1} K_4 \qquad 0.5\,\text{H}_2 + \text{C}^* = \text{CH}^* \quad [24]$$

$$K_{\text{CH}_2} = K_1 K_4 K_5 \qquad \text{H}_2 + \text{C}^* = \text{CH}_2^* \quad [25]$$

$$K_{\text{CH}_3} = K_1^{3/2} K_4 K_5 K_6 \qquad 1.5\,\text{H}_2 + \text{C}^* = \text{CH}_3^*. \quad [26]$$

We may now determine the overall rate of the methanation reaction by solving five equations (namely, $r_3 = r_4 = r_5 = r_6 = r_7$ and site balance) to determine the five unknown values of z_4, z_5, z_6, θ_*, and θ_{c}.

Parameterization of Kinetic Model

The equilibrium constants (K_1, K_2, K_{CH}, K_{CH_2}, K_{CH_3}) required to describe coverages of stable surface species are expressed in terms of the appropriate standard entropy changes (ΔS_1^{o}, ΔS_2^{o}, $\Delta S_{\text{CH}}^{\text{o}}$, $\Delta S_{\text{CH}_2}^{\text{o}}$, $\Delta S_{\text{CH}_3}^{\text{o}}$) and enthalpy changes ($\Delta H_1$, ΔH_2, ΔH_{CH}, ΔH_{CH_2}, ΔH_{CH_3}). The reference pressure for the standard state of gaseous species is 1 atm. The standard entropy changes can be expressed in terms of known gaseous entropies and entropies of appropriate surface species. The combined, quasi-equilibrium constants for the formation of activated complexes ($K_{\text{act3}} - K_{\text{act7}}$) can also be expressed in terms of standard entropy changes ($\Delta S_{\text{act3}}^{\text{o}} - \Delta S_{\text{act7}}^{\text{o}}$) and enthalpy changes ($\Delta H_{\text{act3}} - \Delta H_{\text{act7}}$).

Results from calorimetric studies and sticking coefficient data for H_2 adsorption on Ni(100) indicate that the values of ΔH_1 and ΔS_1^{o} should be near -95 kJ/mol and -86 J/mol/K, respectively (23). Similarly, results for CO adsorption indicate that values of ΔH_2 and ΔS_2^{o} should be near -115 kJ/mol and -95 J/mol/K, respectively (32). The activation barrier for CO dissociation has been measured to be approximately 100 kJ/mol on Ni(111) (1, 13); and the entropy change for dissociation can be estimated to be near -38 J/mol/K, corresponding to a preexponential factor of 10^{11}/s. The results from our quantum chemical calculations are used to provide estimates for the remaining enthalpy changes required in the kinetic model, i.e., ΔH_{CH}, ΔH_{CH_2}, ΔH_{CH_3}, and $\Delta H_{\text{act3}} - \Delta H_{\text{act7}}$. Finally, to obtain initial estimates for the remaining entropy changes of the kinetic model, we assume that each adsorbed species loses 3 degrees of translation upon adsorption and is immobile on the surface; therefore, we initially assume that the entropy of each surface species, including each activated complex, is equal to its local value, S_{loc} ($= S_{\text{gas}} - S_{\text{3D translation}}$). Table 1 shows the initial values of all kinetic parameters.

Description of Methanation Kinetic Data

We now attempt to use our parameterized kinetic model to describe the methanation kinetic data collected by Goodman *et al.* over Ni(100) (1). These experimental data were

TABLE 1

Comparison of Initial Parameters Obtained from Theoretical Studies and Experimental Data and Fitted Parameters Describing the Kinetic Data of CO Methanation

	Initial parameters		Fitted parameters	
Reaction	ΔH (kJ/mol)	ΔS° (J/mol/K)	ΔH (kJ/mol)	ΔS° (J/mol/K)
$\text{H}_2 + 2^* = 2\text{H}^*$	-95	-86	-95	-86
$\text{CO} + * = \text{CO}^*$	-115	-95	-114^a	-86^a
$0.5\,\text{H}_2 + \text{C}^* = \text{CH}^*$	-96	-37	-37^a	14^a
$\text{H}_2 + \text{C}^* = \text{CH}_2^*$	-96	-91	-96	-91
$1.5\,\text{H}_2 + \text{C}^* = \text{CH}_3^*$	-137	-150	-137	-150
$\text{C}^* + \text{O}^* = \text{CO}^{*\ddagger}$	100	-38	84^a	-22^a
$0.5\,\text{H}_2 + \text{C}^* = \text{CH}^{*\ddagger}$	43	-29	43	-29
$\text{H}_2 + \text{C}^* = \text{CH}_2^{*\ddagger}$	-68	-91	-68	-91
$1.5\,\text{H}_2 + \text{C}^* = \text{CH}_3^{*\ddagger}$	-66	-150	-41^a	-141^a
$2\,\text{H}_2 + \text{C}^* = \text{CH}_4^{*\ddagger}$	-93	-234	-91^a	-185^a

[a] Sensitive parameters.

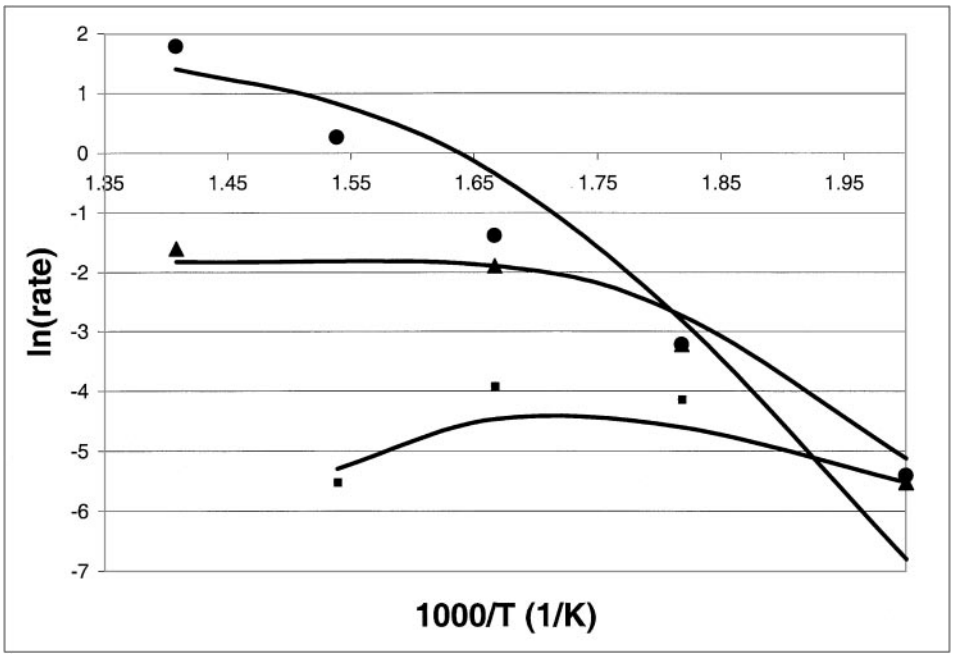

FIG. 5. Arrhenius plot of CO methanation rates on Ni(100), $H_2:CO = 4:1$, $P_{total} = 1$ Torr (■), 10 Torr (▲), and 120 Torr (●). The curves are calculated using the kinetic model.

obtained for a wide temperature range (450–800 K) at total pressures of 1, 10, and 120 Torr, for a fixed $CO:H_2$ ratio equal to 4:1. Methanation is generally regarded as a structure insensitive reaction, and our calculations for the Ni(111) surface should be appropriate to describe the kinetic behavior of the Ni(100) surface studied by Goodman *et al.*

The aim of our kinetic analysis was to assess by how much the kinetic parameters of our model need be changed from their theoretically predicted values to obtain a reasonable fit of the experimental kinetic data. Our fit of the data is shown in Fig. 5, and the values of the fitted kinetic parameters used in our model are presented in Table 1. Importantly, we find in our predicted range of parameter space that there are only five kinetically significant parameters, namely K_2, k_3, K_{act6}, K_{act7}, and K_{CH}. The insensitive parameters (K_1, K_{CH_2}, K_{CH_3}, K_{act4}, and K_{act5}) are arbitrarily fixed at their initial values, as can be seen from Table 1. Because of the compensation effect, a considerable uncertainty exists in the estimation of both enthalpy and entropy changes for each sensitive kinetic parameter. Therefore, we simply report here the 95% confidence limits for the standard Gibbs free energy changes associated with each of the sensitive parameters. In particular, the confidence limits for the Gibbs free energy changes corresponding to K_2, k_3, K_{act6}, and K_{act7} are ± 5 kJ/mol, while the confidence limit for the Gibbs free energy change corresponding to K_{CH} is ± 10 kJ/mol.

The fitted values for the standard entropy and enthalpy changes for CO adsorption and CO dissociation (steps 2 and 3) are very close to the experimental values that we used in the initial parameterization of the model. Our initial estimate for ΔH_{act6} from quantum chemical calculations was -66 kJ/mol, while the fitted value for this parameter was equal to -41 kJ/mol, indicating that the activated complex for step 6 was slightly less stable than estimated from our quantum chemical calculations. Our initial estimate for the standard entropy change ΔS_{act6} was -150 J/mol/K, while the fitted value was equal to -141 J/mol/K, indicating that the activated complex for step 6 possessed some surface mobility. The theoretically predicted value for ΔH_{CH} was -96 kJ/mol, while the fitted value is -37 kJ/mol, indicating that CH^* species were less stable than estimated from our quantum chemical calculations. Also, the standard entropy change ΔS^{o}_{CH} was initially estimated to be -37 J/mol/K, while the fitted value is 14 J/mol/K, indicating that CH^* species possessed some surface mobility.

The aforementioned adjustments we made in the enthalpy changes associated with K_{act6} and K_{CH} to fit the experimental reaction kinetics data were also found to be appropriate for the value of K_{act7}. In particular, the activated complex for step 7 was found to be less stable than estimated from our quantum chemical calculations. Figure 6 shows the quantum chemical and fitted values of electronic energies associated with each stable CH_x species and the corresponding activated complexes. The electronic energies for the kinetically insensitive species are fixed at their quantum chemical values. The largest difference between the fitted and quantum chemical value is associated with methylidyne species. The surface species were found to possess some surface mobility. We note that the two-dimensional

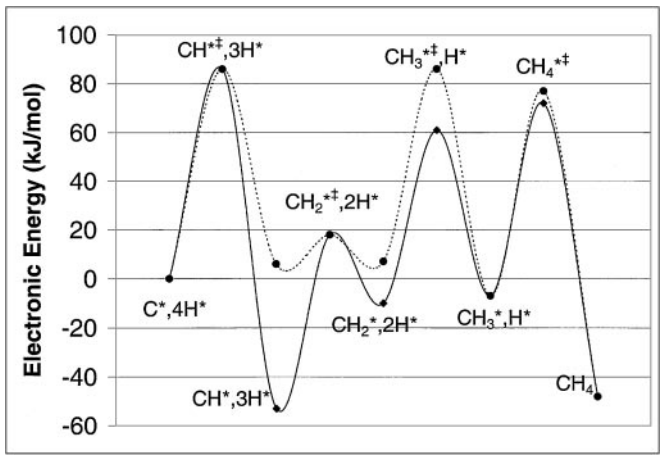

FIG. 6. Electronic energy plot for CH_x species on Ni(111), quantum chemical values (◆) and fitted values (●).

translational entropy for CH_x species, S_{2D}, is near 60 J/mol/K, and the increases in surface entropies from the initial value of S_{loc} suggested by fitting the experimental reaction kinetics data are well within this limiting value of S_{2D}.

The most abundant surface species predicted by the kinetic model are CO^* and CH^*, for the reaction conditions employed by Goodman *et al.*, and Fig. 7 shows the CO^* and CH^* coverages versus temperature at 120 and 10 Torr total pressure. These predictions of the kinetic model are in agreement with a recent mechanistic study of CO methanation on Ni/SiO_2 at atmospheric pressure for a $H_2:CO$ ratio equal to 2 (33), which indicated that the CO coverage on nickel was high (0.88 ML) at 500 K, decreasing to 0.6 ML at 623 K. In addition, the coverage by adsorbed CH_x species was shown to increase with increasing temperature, reaching a value of 0.4 ML at 623 K from 0.08 ML at 500 K. We predict that the methylidyne species (CH^*) is the most abundant hydrocarbon species on the surface, in agreement with previous experimental studies (34, 35). Methylene species (CH_2^*) are also present in small quantities (approximately 0.04). We predict that the surface coverages by other species (C^*, CH_3^*, and H^*) are negligible under the methanation reaction conditions employed by Goodman *et al.*

The results of our kinetic analyses indicate that the value of z_5 is essentially equal to unity under the reaction conditions of Goodman *et al.*, indicating that step 5 is quasi-equilibrated. Accordingly, the rate of the overall reaction is not sensitive to the value of K_{act5}. The value of z_4 is typically equal to 0.1 at lower temperatures, and the value of z_4 approaches unity with increasing temperature. Therefore, step 4 is highly reversible, but not strictly quasi-equilibrated at the reaction conditions considered here. The high reversibility of step 4 is the origin for the low sensitivity of the overall rate with respect to K_{act4}. The value of z_6 is significantly lower than unity under most reaction conditions, indicating that formation of methyl species from methylene species is rather irreversible. We note that we have assumed step 7 to be irreversible. Indeed, if we include the value of z_7 in our analysis, then this value is predicted to be very small.

Figure 8 illustrates the role of different transition states in determining the overall rate of the methanation reaction, as well as in the determining which steps are kinetically significant. This figure shows the Gibbs free energy barriers, $\Delta^{\ddagger}G_i$, associated with the formation of each of the four activated complexes $Act_i^{\ddagger}$. Gas phase dihydrogen and adsorbed

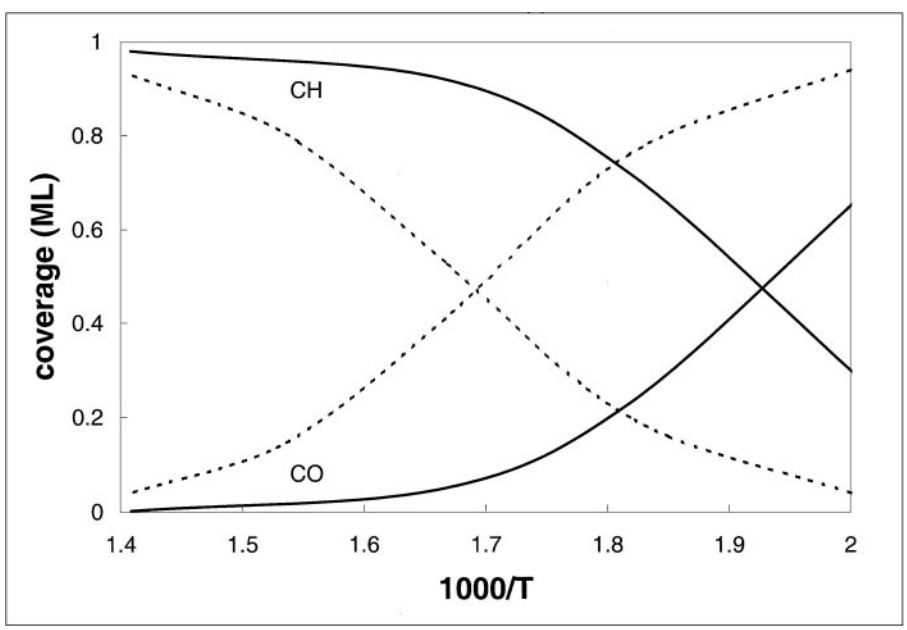

FIG. 7. Coverages of CO and CH predicted by the kinetic model for CO methanation. Dashed lines, $P_{total} = 120$ Torr; solid lines, $P_{total} = 10$ Torr.

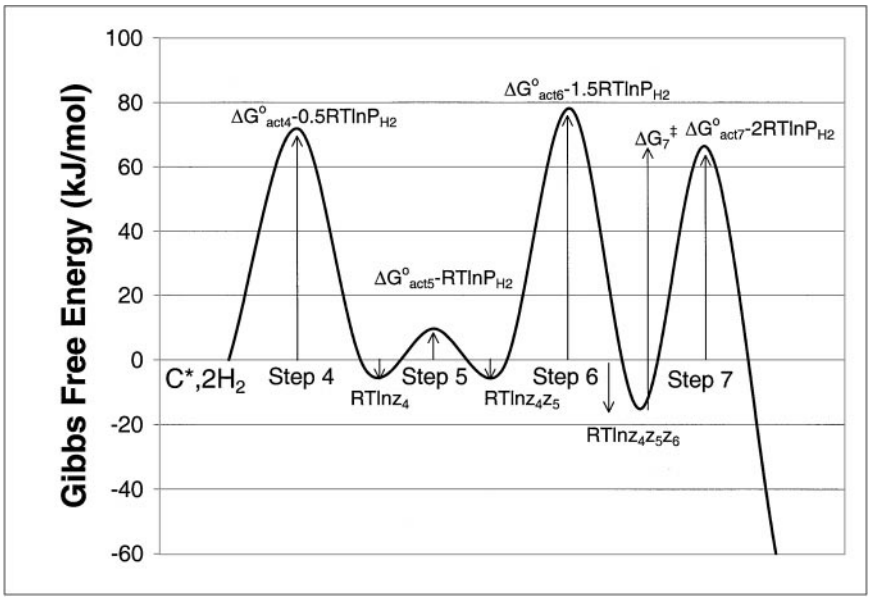

FIG. 8. Gibbs free energy plot for stable species and activated complexes on Ni(111) for CO methanation at $P_{\text{total}} = 10$ Torr and 600 K.

carbon ($2H_2 + C^*$) form the reference for this plot, with an assigned value of zero Gibbs free energy. Table 2 shows the values of $\Delta G^{\circ}_{\text{act},i}$ used to construct the plot in Fig. 8, and it shows the values of z_i, the Gibbs free energy barriers, $\Delta^{\ddagger}G_i$, and the Gibbs free energy changes for steps 4–7 determined from the experimental data of Goodman *et al.* at 600 K and 10 Torr total pressure.

To construct the plot in Fig. 8 of Gibbs free energy, we first determine the change in standard Gibbs free energies for each of the combined, quasi-equilibria that describe the formation of activated complexes from C^* and gaseous H_2. For example, the value of $\Delta G^{\circ}_{\text{act5}}$ is given by

$$\Delta G^{\circ}_{\text{act5}} = G^{\circ}_{\text{act5}} - G^{\circ}_{C^*} - G^{\circ}_{H_2}. \qquad [27]$$

We then note that the rate of step 5 is given by

$$r_5 = K_{\text{act5}} P_{H_2} z_4 \theta_c \theta_* (1 - z_5), \qquad [28]$$

which can be written as

$$r_5 = \nu^{\ddagger} e^{\frac{-1}{RT}\left(\Delta G^{\circ}_{\text{act5}} - RT\ln\left(P_{H_2}\right) - RT\ln z_4\right)} \theta_c \theta_* (1 - z_5). \qquad [29]$$

TABLE 2

Values of Gibbs Free Energies of Activated Complexes and Reactive Intermediates for CO Methanation at 600 K and 10 Torr Total Pressure

Step	z_i	ΔG_i (kJ/mol)	$\Delta G^{\circ}_{\text{act},i}$ (kJ/mol)	$\Delta^{\ddagger}G_{\text{act},i}$ (kJ/mol)
4	0.546	−3	60	72
5	0.999	∼0	−13	13
6	0.087	−12	44	81
7	∼0	Large	20	81

The value $[\Delta G^{\circ}_{\text{act5}} - RT\ln(P_{H_2}) - RT\ln z_4]$ corresponds to a Gibbs free energy barrier, and it is equal to the change in Gibbs free energy for the formation of the activated complex for the fifth step in its standard state, from the reactant C^* in its standard state, and from gaseous H_2 at its temperature and partial pressure in the methanation reactor. Since the Gibbs free energy decreases by $RT\ln(z_4)$ after step 5, we note that the position of the maximum in the plot of Gibbs free energy versus reaction coordinate for step 5 is located at $\Delta G^{\circ}_{\text{act5}} - RT\ln(P_{H_2})$. After conducting similar analyses for the other steps in Fig. 8, we find that the maxima for steps 4, 6, and 7 in the plot of Gibbs free energy versus reaction coordinate are located at $\Delta G^{\circ}_{\text{act4}} - 1/2\,RT\ln(P_{H_2})$, $\Delta G^{\circ}_{\text{act6}} - 3/2\,RT\ln(P_{H_2})$, and $\Delta G^{\circ}_{\text{act7}} - 2\,RT\ln(P_{H_2})$, respectively.

For a particular set of reaction conditions, the values of z_4, z_5, and z_6 are determined by solving the steady state relations ($r_3 = r_4 = r_5 = r_6 = r_7$) and the site balance. We then determine the change in Gibbs free energy, ΔG_i for each step 4, 5, and 6 by the relation

$$\Delta G_i = RT\ln(z_i). \qquad [30]$$

We note that this change in Gibbs free energy, ΔG_i, for a particular reaction step corresponds to the formation the products of that step from the reactants of that step at the temperature, partial pressures, and surface coverages of the reaction conditions. Thus, we plot in Fig. 8 the values of $RT\ln(z_4)$, $RT\ln(z_5)$, and $RT\ln(z_6)$ for methanation reaction at 10 Torr total pressure and at 600 K.

The rates of elementary steps are controlled by their respective Gibbs free energy barriers. As indicated above, the rate of step 5 is controlled by a Gibbs free energy barrier,

$\Delta^{\ddagger}G_5$, equal to $\Delta G^{o}_{act5} - RT\ln(P_{H_2}) - RT\ln(z_4)$. We note that the term $\theta_c\theta_*$ is present in all of the rate expressions for steps 4 through 7; therefore, we need not consider this term in Fig. 8. Also, we note that the $(1-z_i)$ terms in the rate expressions adjust the rates of the steps such that the net rates are equal at steady state. Thus, a step with a low Gibbs free energy barrier has a value of z_i that is near unity.

Figure 8 shows that the highest Gibbs free energy barriers are involved in the formation of activated complexes 6 and 7, leading to high sensitivities of the overall rate on the kinetic parameters K_{act6} and K_{act7}. While the Gibbs free energy barrier for step 4 is significant, its value is lower than for steps 6 and 7; therefore, the overall rate is not very sensitive to the value of K_{act4}. Finally, the Gibbs free energy barrier for step 5 is very low, and the overall rate is not sensitive to the kinetic parameters K_{act5}.

DISCUSSION

As mentioned earlier we have reported the energy values for various species obtained by using the RPBE functional. Table 3 compares these values with those obtained by using the PW-91 functional. We find that the PW-91 functional overpredicts the binding energies for surface species in accord with an earlier report (19). The comparison between the energetics obtained from the two functionals may be an indictor of the uncertainty in the theoretical predictions.

We compare in Table 4 our energetics with some representative theoretical studies in the literature. Au *et al.* have conducted DFT calculations on a 7-atom Ni cluster (4), van Santen and coworkers have carried out DFT calculations on a 13-atom cluster (6), Yang and Whitten have used an embedded cluster approach on a three-layer 62-atom cluster (10), while Panas and Siegbahn have used a "bond preparation" method on a 10- and 25-atom cluster (8). Au *et al.* have used a bond-order conservation Morse potential approach to evaluate the activation energies. There is fairly good agreement between our results and those of Au *et al.* in terms of the energetics for all steps, except the last step which is the associative desorption of methane. However, Au *et al.* predict an atop site to be favored by adsorbed methyl group, as found by Burghgraef *et al.* (6). Our results show that the methyl group has a strong preference for the threefold site, in agreement with spectroscopic data and other theoretical studies (9, 12).

From the calculations presented here we conclude that the activation barrier for methane dissociation on Ni(111) surface is 127 kJ/mol. In an earlier theoretical study from our group, we found an activation barrier of 109 kJ/mol (7). However, the former study used the PW-91 GGA exchange-correlation functional, while in the present paper we have used the RPBE functional. Furthermore, the former study used a calculated LDA equilibrium lattice constant that is 0.05 Å shorter than the lattice constant used in the present work. Also, the former study used a self-consistently calculated LDA density as input into the GGA functional, which can lead to errors in the non-self-consistent energy. The calculated barrier of the present study agrees with results of molecular beam studies (36) but appears to be somewhat higher than reported from sticking coefficient experiments (37, 38). One possibility is that the latter experiments are dominated by adsorption at steps and other defects. Ongoing calculations in our group for the barrier for CH_4 dissociation at a step on Ni(211) give a barrier much closer to the experimentally determined value.

Ceyer and coworkers have identified a loss feature at 485 cm^{-1} to be the torsional mode for adsorbed CH_3 on Ni(111) (12). Our calculations show a barrier of 33 kJ/mol for the torsional motion of methyl species. This high barrier is in agreement with the high frequency of this torsional motion. The methyl dissociation product produced by raising the temperature of the Ni surface from 80 to 220 K was found to be adsorbed CH species and adsorbed H atoms. The onset of this conversion is reported to be at 150 K. No CH_2 species were observed during the reaction. Ceyer and coworkers have attributed the absence of CH_2 species to the inability to trap these species at the temperatures required to dissociate CH_3 (12). Our calculations are in agreement with this explanation. The activation energy to

TABLE 3

Effect of the Density Functional (RPBE versus PW-91) on the Calculated Electronic Energies of Elementary Steps

Reaction	RPBE energy (kJ/mol)	PW-91 energy (kJ/mol)
$H_2 + 2^* = 2H^*$	−86	−123
$C + * = C^*$	−613	−662
$C^* + H^* = CH^* + *$	−53	−43
$CH^* + H^* = CH_2^* + *$	43	52
$CH_2^* + H^* = CH_3^* + *$	3	12
$CH_3^* + H^* = CH_4 + 2^*$	−41	18

TABLE 4

Comparison of the Electronic Energies in the Present Work with Previously Reported Theoretical Calculations

Reaction	Energy (kJ/mol)				
	Present study	(4)	(6)	(10)	(8)
$C^* + H^* = CH^{*\ddagger}$	86	93			
$C^* + H^* = CH^*$	−53	−23	−27		50
$CH^* + H^* = CH_2^{*\ddagger}$	71	136			
$CH^* + H^* = CH_2^*$	43	68	27	−140	−29
$CH_2^* + H^* = CH_3^{*\ddagger}$	71	96			
$CH_2^* + H^* = CH_3^*$	3	19	−24	−55	−58
$CH_3^* + H^* = CH_4^{*\ddagger}$	86	73			
$CH_3^* + H^* = CH_4$ (g)	−41	23	−30	−4	48

form CH_2 from CH_3 is higher than the activation energy to form CH from CH_2. In experimental studies, the reaction $CH_3(ads) = CH(ads) + 2H(ads)$ is found to be exothermic, and we find this reaction to be exothermic by 46 kJ/mol.

Methane formation was not observed from low coverages (ca. 0.05 ML) of methyl groups on Ni(111), even in the presence of considerable coadsorbed hydrogen (39). On the other hand, at higher coverages (0.3 ML) methane is formed at 235 K by the reaction of surface hydrogen atoms with methyl groups on Ni(111) (40, 41). Our reaction energy diagram is in good agreement with this observation. The activation barriers to form methane or methylene from methyl group are similar (86 and 68 kJ/mol, respectively). Hence, adsorbed methyl groups may form methane at high coverage or dissociate to methylene (and further to methylidyne) at low coverage when empty sites are available to accommodate hydrogen.

We find that the work function of Ni decreases upon adsorption of CH_x species. Experimentally, chemisorption of organic molecules on transition metals usually decrease the work function. In particular, adsorption of methane, ethane, propane, ethylene on polycrystalline Pt (42), ethylene adsorption on thin films of Ni, Pd, and Pt (43), and adsorption of methane and ethane on Pt foil (44) have been studied by changes in work function. The decrease in the work function indicates that electrons are transferred from the adsorbed hydrocarbon species toward the metal, and the adsorbed species assumes a positive charge. In contrast to these results, previous cluster calculations of CH_4 dissociation on Ni have shown that the adsorbed CH_3 species have a net negative charge. In particular, Yang and Whitten report a net negative charge of 0.4 e on methyl species and a work function increase of 0.26 eV upon adsorption of methyl species (9). A recent cluster calculation of adsorbed CH_3 on Ni also predicts electron transfer from the metal to the CH_3 group (4). A DFT study of acetylene and ethylene adsorption on Ni(111) also predicts that adsorbed species have a net negative charge (45). These analyses are based on Mulliken populations, where it is assumed that the overlap population can be equipartitioned between the two contributing basis functions. In general, cluster calculations do not predict the experimentally observed direction of charge transfer upon adsorption of hydrocarbons on metal surfaces. Agreement with the experimental work function measurements seems to be an important strength of the slab approach over the cluster approach.

We have shown how De Donder relations can be used to express the overall rate of the reaction in terms of quasi-equilibria between the reactants and/or products of overall reaction with the transition states of the elementary steps, and the fraction of the surface that is available for reaction is expressed by equilibria between the reactants and/or of overall reaction with the abundant surface adsorbed species. The combined kinetic parameters that are identified in this manner are convenient for assessing the sensitivities of the factors that control the rate of the overall reaction. The results of our analyses for methanation over nickel suggest that CO^* and CH^* are the most abundant surface species for the reaction conditions employed by Goodman *et al.* Therefore, the kinetic parameters controlling the coverages of these species (namely K_2 and K_{CH}) are sensitive for prediction of the overall rate of methanation. We find that the fitted value of the enthalpy change for K_{CH} is more endothermic than the theoretically predicted value. We note that we have not taken into account the stabilization of surface carbon caused by surface reconstruction, which was calculated to be near 20 kJ/mol in a separate theoretical study. Also the binding energy of CH^* is expected to be lower at higher coverages. Both these factors can explain the more endothermic values obtained from the fit to the kinetic data. We also note that the energies obtained from quantum chemical calculations do not include zero point energy and thermal corrections. We find that all surface species have some fraction of two-dimensional translational entropy.

Our kinetic analyses indicate that the energies of the transition states to form methyl species from methylene species ($Act_6^\ddagger$) and to form methane from methyl species ($Act_7^\ddagger$) are critical to predict the rate of the overall reaction. The remaining two transition states described in this paper ($Act_4^\ddagger$ and $Act_5^\ddagger$) do not appear to affect the rate of methanation at the reaction conditions employed by Goodman *et al.* This conclusion can be seen from Fig. 8. We note that K_{act3}, which is equal to K_2k_3, has a negative temperature dependence, since $\Delta H_2 = -114$ kJ/mol and $\Delta^\ddagger H_3 = 84$ kJ/mol. This negative temperature dependence results in the rate curves bending down at higher temperature, in agreement with experimental data. This reaction scheme does not have a single rate limiting step. As shown by Boudart (29), the existence of a rate limiting step requires that one and only one value of z_i should be small, with all other values of z_i equal to unity.

We note that it is difficult to describe reaction kinetics data collected over a wide range of temperatures and pressures using a single set of kinetic parameters. For example, Langmuirian kinetics may not be appropriate when the surface coverages change significantly. In addition, the calculated energy changes do not include lateral interactions and the parameters obtained may depend on the coverage. Thus, the aim of this study is not to achieve a detailed description of the kinetic data, but rather to show how theoretical results can be combined with De Donder analysis to obtain a reasonable description of the catalytic system. Importantly, this approach presents a means to identify natural groups of parameters that allow the reaction kinetics to be described in terms of combined, quasi-equilibria involving activated complexes, abundant surface species, and the gaseous reactants and/or products of the overall reaction.

We note that even though methanation is generally regarded as a structure-insensitive reaction, its rate has been shown to depend on the particle size much more than can be explained by the change in surface area on supported Ni catalysts (2). Hence the present analysis may not be valid for all reaction conditions.

CONCLUSIONS

We have used a plane wave slab approach in conjunction with density functional theory to investigate the energetics of surface reactions of methane on Ni(111). The predicted structures of various surface CH_x species ($x = 1, 2, 3$) are in good agreement with available spectroscopic data. For example, the methyl group is shown to prefer a threefold site. In fact, all CH_x species prefer threefold sites on Ni(111). The predicted relative energies are also in agreement with experimental observations. We report the activation barriers obtained from first principles for C–H bond activation of these species. We demonstrate the good agreement of our theoretical results with work function measurements.

We have consolidated our theoretical results and available experimental data to formulate a kinetic model to explain CO methanation kinetics on the Ni(100) surface. The energetics from the quantum chemical treatment of the system provide an initial estimate of all kinetic parameters. Sensitivity analyses were conducted to determine the effects of these parameters on the overall rate of methanation. The sensitive parameters were then systematically adjusted to describe the experimental data, namely the kinetics and the experimental observations of the abundant surface species.

We have shown that De Donder relations provide a simple means to determine the number of kinetic parameters required to calculate the overall reaction rate from a reaction scheme. These parameters may be termed as 'natural' parameters, since they contain a systematic combination of various equilibrium constants. We illustrate how these natural parameters are controlled by quasi-equilibria between the reactants and/or products of the overall reaction with the transition states of elementary steps, and they are not determined by the properties of stable reaction intermediates. The rate also depends on the coverages of the abundant, stable surface species, which are predicted to be adsorbed CO and CH. We find that there is no single rate limiting step for the reaction scheme.

ACKNOWLEDGMENTS

One of the authors (R.M.W.) thanks Haldor Topsøe A/S for arranging an internship and Foster Foundation for a travel fellowship. We thank Bjerne Clausen, Ib Alstrup, and Joachim Jacobsen for stimulating discussions. We thank Lars Hansen for help with the density functional total energy program.

REFERENCES

1. Goodman, D. W., Kelley, R. D., Madey, T. E., and Yates, J. T., Jr., *J. Catal.* **63**, 226 (1980).
2. Rostrup-Nielsen, J. R., *in* "Catalysis, Science and Technology" (J. R. Anderson and M. Boudart, Eds.), Springer-Verlag, Berlin, 1984.
3. Ponec, V., *Catal. Rev. Sci. Eng.* **18**, 151 (1978).
4. Au, C., Liao, M., and Ng, C., *J. Phys. Chem. A* **102**, 3959 (1998).
5. Baetzold, R. C., *J. Phys. Chem.* **88**, 5583 (1984).
6. Burghgraef, H., Jansen, A. P. J., and van Santen, R. A., *Surf. Sci.* **324**, 345 (1995).
7. Kratzer, P., Hammer, B., and Norskov, J. K., *J. Chem. Phys.* **105**(13), 5595 (1996).
8. Siegbahn, P. E. M., and Panas, I., *Surf. Sci.* **240**, 37 (1990).
9. Yang, H., and Whitten, J. L., *J. Am. Chem. Soc.* **113**, 6442 (1991).
10. Yang, H., and Whitten, J. L., *Surf. Sci.* **255**, 193 (1991).
11. Kaminsky, M. P., Winograd, N., Geoffrey, G. L., and Vannice, M. A., *J. Am. Chem. Soc.* **108**, 1315 (1986).
12. Yang, Q. Y., Maynard, K. J., Johnson, A. D., and Ceyer, S. T., *J. Chem. Phys.* **102**, 7734 (1995).
13. Kelley, R. D., and Goodman, D. W., *Surf. Sci.* **123**, L743 (1982).
14. Dumesic, J. A., *J. Catal.* **185**, 496 (1999).
15. Vanderbilt, D. H., *Phys. Rev. B* **41**, 7892 (1990).
16. Perdew, J. P., *et al., Phys. Rev. B* **46**, 6671 (1992).
17. White, J. A., and Bird, D. M., *Phys. Rev. B* **50**, 4954 (1994).
18. Kresse, G., and Furthmuller, J., *Comput. Mat. Sci.* **6**, 15 (1996).
19. Hammer, B., Hansen, L. B., and Norskov, J. K., *Phys. Rev. B* **59**, 7413 (1999).
20. Khein, A., Singh, D. S., and Umrigar, C. J., *Phys. Rev. B* **51**, 4105 (1995).
21. Christmann, K., Schober, O., Ertl, G., and Neumann, M., *J. Chem. Phys.* **60**, 4528 (1974).
22. Christmann, K., Behm, R. J., Ertl, G., van Hove, M. A., and Weinberg, W. H., *J. Chem. Phys.* **70**, 4168 (1979).
23. Christmann, K., *Surf. Sci. Rep.* **9**, 1 (1988).
24. Klinke, D. J., Wilke, S., and Broadbelt, L. J., *J. Catal.* **178**, 540 (1998).
25. Klink, C., Stensgaard, I., Besenbacher, F., and Laegsgaard, E., *Surf. Sci.* **342**, 250 (1995).
26. Alstrup, I., *J. Catal.* **151**, 216 (1995).
27. De Donder, T., "L'Affinite," p. 43. Gauthier-Villers, Paris, 1927.
28. Boudart, M., *J. Phys. Chem.* **87**, 2786 (1983).
29. Boudart, M., *Catal. Lett.* Submitted for publication.
30. Laidler, K. J., "Chemical Kinetics," 3rd ed. Harper Collins, New York, 1997.
31. Laidler, K. J., and King, M. C., *J. Phys. Chem.* **87**, 2657 (1983).
32. Al-Sarraf, N., Stuckless, J. T., Wartnaby, C. E., and King, D. A., *Surf. Sci.* **283**, 427 (1993).
33. Agnelli, M., Swaan, H. M., Marquez-Alvarez, C., Martin, G. A., and Mirodatos, C., *J. Catal.* **175**, 117 (1998).
34. Happel, J. H., *et al., J. Catal.* **73**, 314 (1982).
35. Hayes, R. E., Thomas, W. J., and Hayes, K. E., *J. Catal.* **92**, 312 (1985).
36. Holmblad, P. M., Larsen, J. H., and Chorkendorff, I., *J. Chem. Phys.* **104**, 7289 (1996).
37. Beebe, T. P., Goodman, D. W., Kay, B. D., and Yates, J. T., *J. Chem. Phys.* **87**, 2305 (1987).
38. Chorkendorff, I., Alstrup, I., and Ullmann, S., *Surf. Sci.* **227**, 291 (1990).
39. Johnson, A. D., Dley, S. P., Utz, A. L., and Ceyer, S. T., *Science* **257**, 223 (1992).
40. Hall, R. B., Castro, M., Kim, C. M., and Mims, C. A., *Stud. Surf. Sci. Catal.* **101**, 327 (1996).
41. Tjandra, S., and Zaera, F., *J. Catal.* **147**, 598 (1994).
42. Hlavathy, Z., Tetenyi, P., and Paal, Z., *J. Chem. Soc. Faraday Trans.* **88**(14), 2059 (1992).
43. Franken, P. E. C., and Ponec, V., *Surf. Sci.* **53**, 341 (1975).
44. Hlavathy, Z., and Tetenyi, P., *React. Kinet. Catal. Lett.* **62**, 163 (1997).
45. Fahmi, A., and van Santen, R. A., *Surf. Sci.* **371**, 53 (1997).